II.2 Techniques Based on Photons and Other Probes

10. Surface Structure by X-Ray Diffraction

I.K. Robinson
AT&T Bell Laboratories, Murray Hill, NJ 07974, USA

The diffraction of X-rays by crystalline matter has been well understood for 60 years. In that period a vast amount of practical expertise, in the form of X-ray crystallography, has been developed for the determination of crystal structures on the atomic scale. Low-energy electron diffraction (LEED) has extended crystallography to include crystal surfaces, but, as some of the accompanying papers have shown, data analysis is not so straightforward because of multiple scattering and the need for accurate atomic models. Neither of these is a serious problem in X-ray structure analysis.

The X-ray intensity scattered from a crystal is easily calculated by summing the contribution of every electron in the sample using the Thomson formula [10.1]. When applied to a monolayer at the surface of a crystal (or, equivalently, a reconstructed surface or other 2D arrays of atoms) with typical sources and instruments, the numbers in Table 10.1 result. The first lesson is that X-ray experiments with single monolayers are indeed practical. It is clear that under favorable choice of system, a conventional laboratory source is sufficient but for more general problems synchrotron radiation is needed.

Table 10.1. Calculated signal rates for the two reconstructed surfaces of interest to this paper. Approximate primary beam intensities (monochromatic) delivered to a typical sample are compared for conventional and synchrotron sources. The calculated diffraction signals assume a perfect 2D array of atoms, one per unit cell

Source	Primary beam Photons/s	Diffracted from Au(110) 2×1 Photons/s	Diffracted from Si(111) 7×7 Photons/s
60 kW Rotating anode	10^{8}	10	10^{-4}
SSRL bending magnet	10^{11}	10^{4}	10^{-1}
SSRL wiggler magnet	10^{12}	10^{5}	1
SSRL 54-pole wiggler	10^{13}	10^{6}	10

In proceeding to find the optimum experimental geometry, we must consider the function of an X-ray diffractometer. Conventionally, the detector and source direction lie in a "diffraction plane" fixed in space. The X rays are highly collimated within the plane but poorly normal to it. This gives rise to a resolution function which is highly asymmetric with the long direction normal to the diffraction plane [10.2]. The diffraction pattern of the 2D sample is an array of "rods", sharp in the direction parallel to the surface plane, but diffuse normal to it. Clearly the largest convolution of this pattern with the resolution function is when both long directions are aligned. Thus the surface plane is parallel to the diffraction plane with the incident and diffracted rays at glancing angle. This "glancing incidence" geometry [10.3] has another useful feature: the depth of penetration into the bulk is drastically reduced and so, therefore, is the thermal diffuse background upon which the surface signal sits.

Experimentally, a UHV preparation apparatus, a full 4-circle X-ray diffractometer and high-power X-ray source are required. Specific technical problems are the design of UHV-compatible X-ray windows and a means of precision (0.001°) sample manipulation [10.4]. Published work using the technique in recent years includes Ge(100) [10.5] and Au(110) [10.6] reconstructed surfaces as well as Pb/Cu(110) [10.7] and Xe/Graphite [10.8] adsorption systems. The high-resolution capabilities and the ability to determine atomic structures have been demonstrated. Much work is in progress and a large number of groups are adopting the technique. Some prospective areas of interest are crystal/crystal and crystal/liquid interfaces, 2D melting and phase transitions, nucleation and growth of overlayers and magnetic ordering at surfaces. The remainder of this paper is devoted to recent results on surface reconstructions that will serve as examples.

10.1 Observation of Domain Wall Structures in Au(110)

The structure of the reconstructed Au(110) surface has been previously reported [10.6,9]. Superlattice reflections were found close to half order positions along (100). A 2×1 missing row structure, in which every second row of atoms in the surface layer was absent, was derived by analysis of relative intensities. Pairwise displacements of 0.12 Å were found in the second layer, and this was confirmed by analysis of ion scattering data [10.10]. There was a systematic displacement of the peaks parallel to (100) which varied substantially from sample to sample (Fig.10.1), and was explained in terms of a distribution of domain walls that interrupted the coherence of the surface layer along (100). We proposed monoatomic steps in the surface as a suitable form of walls, consistent with scanning tunneling electron images of Au(110) [10.11].

We have recently succeeded in explaining the observed diffraction line shapes in Fig.10.1 with a suitably "random" distribution of these step domain walls. The absence of wall-wall interaction energy implies the probability of finding a wall is independent of whether it follows another wall or not. We model the Au(110) surface (following [10.9]) by assuming that the predominant structural units are monatomic steps with probability p and 2×1 missing row units with probability (1-p), as shown in Fig.10.2c. This is transformed into a 1-dimensional lattice model by indexing the structure with one site every *half* unit cell as shown in Fig.10.2d and writing the probability of a nearest-neighbor atom m sites away as P_m with

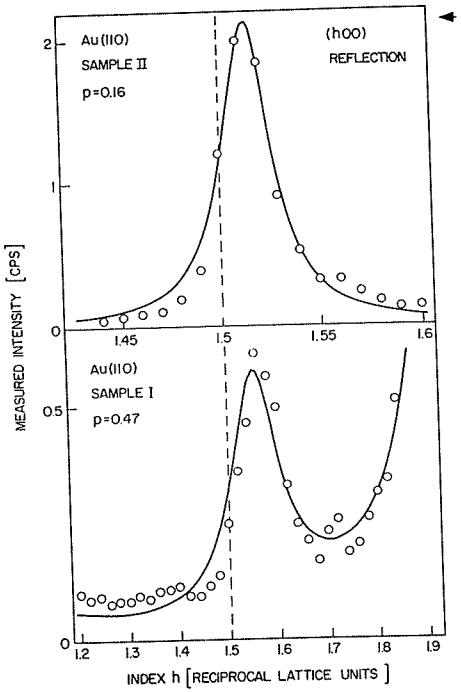

Fig.10.1. Observed diffraction line shapes for two preparations of the Au(110) reconstructed surface [10.6]. A 60 kW rotating anode source and graphite-resolution diffractometer were used. The data were fitted, as described in the text, with the values of step density (p) indicated

Fig.10.2

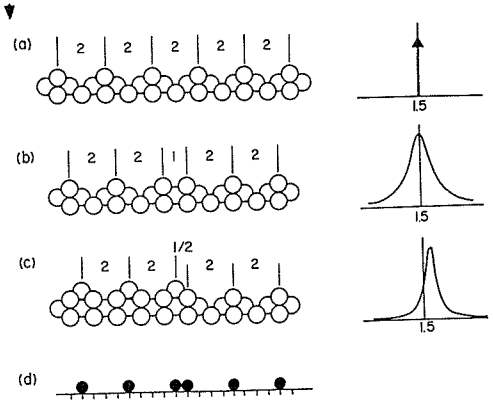

Fig.10.2a-d. Calculated radial diffraction profiles near the (3/2,0,0) superlattice reflection for models of Au(110) surfaces. Repeat spacings are indicated in units of the Au lattice constant, 4.0 Å. (a) Perfect missing-row structure. (b) Missing-row structure with random antiphase boundaries. (c) Missing-row structure with random monatomic steps. (d) Abstraction of structure in (c) to a 1D lattice model, with the allowed sites marked by ticks. The model does not specify whether the steps are up or down, so their density is not constrained externally

$$P_1 = p \quad ,$$

$$P_2 = P_3 = P_{m>4} = 0 \quad ,$$

$$P_4 = (1-p) \quad .$$

This model obeys the definition of "random" above.

If there is an atom at site m = 0 then the cumulative probability of finding an atom at site m is

$$Q_m = \frac{1}{m!}\frac{\partial^m}{\partial x^m}\frac{1}{1-px-(1-p)x^4}\bigg|_{x=0} \quad ,$$

using the generator formalism. The structure factor is then simply the Fourier transform of Q_m which reduces exactly to

$$F(q) = \sum_{m=0}^{\infty} Q_m e^{iqm} = \frac{1}{1-p\,e^{iq}-(1-p)e^{4iq}} \quad . \qquad (10.1)$$

This functional form, which is similar to that calculated for random stacking faults in crystals [10.12], and its analogues for other types of domain walls have been evaluated and compared with observation. As found in [10.9], only the step domain wall of Fig.10.2c explains the observed diffraction peak positions. A counterexample is shown in Fig.10.2b.

Fits of (10.1) to the diffraction data are shown in Fig.10.1. In Figure 10.1 (upper), only the step density p and a scale factor were adjusted for agreement; in Fig.10.1 (lower) the range of momentum transfer was so large that thermal diffuse scattering (Δq^{-2}) around the (200) bulk Bragg peak had to be included as well. The resulting values of step density were p = 0.16 and 0.47, corresponding to average interstep spacings of 52 Å and 18 Å respectively. The slight systematic deviation of the calculated curve from the data in Fig.10.1b is probably due to repulsive interaction between the domain walls.

10.2 First Observation of X-ray Diffraction from Si(111)7 × 7

This is the prototypical example of the phenomenon of surface reconstruction, and was historically the first known case [10.13]. Because of quadratic dependence of the scattering intensity both on the atomic number of the scattering atom and on the unit cell area, the expected signal rates here are 10^5 times smaller than for Au(110). This necessitates the use of a storage ring source of X-rays (Table 10.1).

In collaboration with P. Fuoss and J. Stark of AT&T Bell Labs and P. Bennett of Arizona State University, we report diffraction from this surface seen at the Stanford Synchrotron Radiation Laboratory (SSRL). The surface was prepared by resistive heating to 1450 K in 10^{-10}Torr and was studied using the glancing incidence X-ray geometry on the focused wiggler beam line (VII-2).

Under parasitic running conditions, we surveyed a number of the 1/7th order reflections characteristic of the 7 × 7 reconstruction. The most intense one found was at the (1,3/7) position using the 2D hexagonal nomenclature of LEED or (34/21,-26/21,-8/21) in Miller index notation; this yielded 40 counts per second. The in-plane diffraction profiles (Fig.10.3, insert) were sharp, but still 50% broader than resolution. The surface coherence length was about 6000 Å, in agreement with other observations of the annealed surface [10.14,15].

Structural information normal to the surface is contained in the "rod profiles" of the superlattice reflections. These were measured by tilting the sample an angle χ about a direction bisecting the incident and diffracted beams [10.6], thereby adding a perpendicular component ($q_\perp$) to the in-plane momentum transfer ($q_\parallel$). A typical profile is shown in Fig.10.3. The solid line in Fig.10.3 is the dependence of the profile expected from resolution considerations mentioned in the introduction: the instrumental resolution function is approximated as a prolate ellipsoid with a 200:1 axial ratio (from the collimation angles of the diffractometer) which is aligned with the rod only at $q_\perp = 0$. As $q_\perp$ increases, the rod tilts with respect to the ellipsoid and the intersected length σ varies as

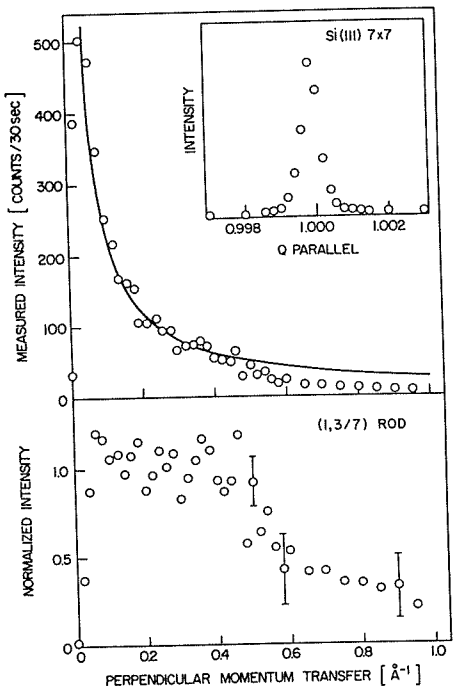

Fig.10.3. *Above*: Diffraction profile of the (1,3/7) superlattice reflection from the Si(111)7 × 7 surface perpendicular to the surface. The solid line is the variation of the width of the resolution function, $\sigma(q_\perp)$ from (10.2). The parallel component of momentum transfer for this reflection is $q_0 = 2.40$ Å^{-1}, so the sample tilts from $\chi = 0$ to $\chi = 22^\circ$ over the range of the scan. *Below*: the same data normalized to $\sigma(q_\perp)$. Insert: radial diffraction profile of the (1,3/7) reflection. The ordinate is in units of q_0

$$\frac{1}{\sigma^2} = \frac{1}{a^2} + \sin^2\chi\left(\frac{1}{b^2} - \frac{1}{a^2}\right) \quad ,$$

$$\tan\chi = \frac{q_\perp}{q_\parallel} \quad , \qquad (10.2)$$

where $a = 2^\circ$ and $b = 0.01^\circ$ are the major and minor axes of the ellipsoid. Figure 10.3 shows that the observed scattering falls below this form at large $q_\perp$ values, and when normalized to it (Fig.10.3 lower) shows a smooth variation. The depth of the reconstruction, which is inversely related to the half-width of the rod, is estimated from the normalized profile to be about 10 Å, or 3 silicon layer spacings.

In-plane structural information is contained in the relative intensities of the different 1/7 order reflections. We measured 30 positions including some symmetry equivalents; the reproducibility was only 30%, and it was clear that a better understanding of the relation between resolution function and sample alignment would be necessary to obtain 1% accuracy. There is, however, excellent *qualitative* agreement between these data and published transmission electron diffraction photographs of Si(111)7 × 7 [10.16].

Finally, we followed the departure of long-range order through the 7 × 7 to "1 × 1" order-disorder transition at 1100 K, as shown in Fig.10.4. We found the transition to be very sharp, with no evidence of residual scattering beyond. We saw no evidence of hysteresis or irreversible behavior.

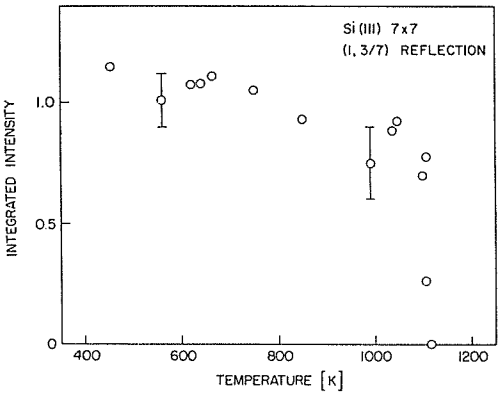

Fig.10.4. Temperature dependence of the integrated (1, 3/7) intensity. Low temperatures were measured from the silicon lattice constant; high temperatures (over 1000 K) were measured by optical pyrometry. In both cases the precision is about ±5 K and the accuracy ±20 K. The error bars on intensity values arise from misalignment

References

10.1 B.E. Warren: *X-ray Diffraction* (Addison Wesley, Reading 1969)
10.2 D.E. Moncton, G.S. Brown: Nucl. Inst. Meth. **208**, 579 (1983)
10.3 W.C. Marra, P. Eisenberger, A.Y. Cho: J. Appl. Phys. **50**, 6927 (1979)
10.4 P.H. Fuoss, I.K. Robinson: Nucl. Inst. Meth. **222**, 171 (1984)
10.5 P. Eisenberger, W.C. Marra: Phys. Rev. Lett. **46**, 1081 (1981)
10.6 I.K. Robinson: Phys. Rev. Lett. **50**, 1145 (1983)
10.7 W.C. Marra, P.H. Fuoss, P. Eisenberger: Phys. Rev. Lett. **49**, 1169 (1982)
10.8 K. D'Amico, D.E. Moncton: To be published
10.9 I.K. Robinson, Y. Kuk, L.C. Feldman: Phys. Rev. B**29**, 4762 (1984)
10.10 Y. Kuk, L.C. Feldman, I.K. Robinson: Surf. Sci. **138**, L168 (1984)
10.11 G. Binning, H. Rohrer, C. Gerber, E. Weibel: Surf. Sci. **131**, L379 (1983)
10.12 A. Guinier: *X-ray Diffraction* (Freeman, San Francisco 1963)
10.13 R.E. Schlier, H.E. Farnsworth: J. Chem. Phys. **30**, 917 (1959)
10.14 M. Henzler: Surf. Sci. **132**, 82 (1983)
10.15 Y. Tanishiro, K. Takayanagi, K. Yagi: Ultramicroscopy **11**, 95 (1983)
10.16 K. Takayanagi, Y. Tanishiro, M. Takahashi, H. Motoyoshi, K. Yagi: Proc. 10th Int. Cong. on Elec. Micros. (Frankfurt 1982)